RESEARCH ARTICLE | MARCH 12 2024

High-fidelity correspondence imaging in complex media with varying thresholds and 1-bit compressive sensing ⊘

Zhihan Xu ⓘ ; Qian Song ⓘ ; Wen Chen ✉ ⓘ

Check for updates

View Online

Export Citation

Applied Physics Letters

High-fidelity correspondence imaging in complex media with varying thresholds and 1-bit compressive sensing

View Online   Export Citation   CrossMark

Zhihan Xu,[1] (iD) Qian Song,[1] (iD) and Wen Chen[1,2,a)] (iD)

AFFILIATIONS

[1]Department of Electrical and Electronic Engineering, The Hong Kong Polytechnic University, Hong Kong, China
[2]Photonics Research Institute, The Hong Kong Polytechnic University, Hong Kong, China

[a)]Author to whom correspondence should be addressed: owen.chen@polyu.edu.hk

ABSTRACT

Here, we report high-fidelity correspondence imaging (CI) in complex media. By introducing varying thresholds to binarize single-pixel light intensities recorded in complex media, dynamic scaling factors can be eliminated. Then, the binarized light intensities and illumination patterns can be fed into a modified 1-bit compressive sensing algorithm to realize high-fidelity object reconstruction. The proposed method can implement object reconstruction with high fidelity in complex media without extra temporal carriers. It is experimentally verified that the method can effectively eliminate dynamic scaling factors and realize high-fidelity object reconstruction in complex media where conventional CI methods could fail. Experimental results demonstrate that the proposed method broadens a potential application of CI in complex media, e.g., turbid water, biological tissues, and dynamic smoke.

Published under an exclusive license by AIP Publishing. https://doi.org/10.1063/5.0198173

Ghost imaging (GI)[1,2] retrieves spatial information of an unknown object from light intensities recorded by a single-pixel detector. As a novel imaging method, GI has shown superior performance beyond pixelated-detector-based imaging methods with the wider working spectrum and higher detection sensitivity.[3] With its advantages, GI has been adopted in various applications, such as microscopy,[4,5] phase imaging,[6,7] optical encryption,[8] and quantum imaging.[9,10] Instead of directly correlating light intensities with illumination patterns, correspondence imaging (CI)[11] has been developed to binarize the intensities with a constant threshold, i.e., an average value of the recorded light intensities. After illumination patterns are separated into two groups based on the binarized intensities, CI implements object reconstruction by simply superimposing illumination patterns belonging to the same group. Compared with GI, CI features efficient reconstruction with higher robustness against non-linear distortions.[12]

Recently, imaging through complex media has attracted increasing attention because of its extensive applications, such as biomedical imaging[13–16] and remote sensing.[17,18] By collecting photons without considering their actual paths, GI shows high robustness against turbulence in scattering media for object reconstruction.[19–22] However, effective reconstruction in GI relies heavily on the assumption of constant scaling factors. When complex media become dynamic, the

scaling factors will change continuously during the measurements, leading to additional fluctuations in the recorded intensities. Xiao *et al.*[23] proposed a method to compensate for the fluctuations by introducing a fixed temporal carrier throughout the measurement, which is time-consuming. Although CI is insensitive to non-linear distortions, most work focuses on its applications in free space where the scaling factors bring only a few fluctuations. In complex media, dynamic scaling factors could fail object reconstruction if the constant threshold is still used for the binarization operation. In addition, object reconstruction based on CI suffers from poor quality according to a probability theory,[24] which limits its applications in complex media.

In this Letter, we report high-fidelity CI in complex media with varying thresholds and 1-bit compressive sensing. To eliminate dynamic scaling factors in complex media, light intensities are binarized with varying thresholds. After the binarization, object information can be retrieved from the binarized intensities and illumination patterns by a modified 1-bit compressive sensing algorithm. Experimental results verify that the proposed method can realize object reconstruction with high fidelity in complex media where conventional methods cannot work. Compared with the temporal correction approach, the proposed method requires no temporal carriers and maintains good performance under low sampling ratios. Our approach opens broad

prospects for CI with potential applications in various complex media, such as biological tissues, turbid water, and dynamic smoke.
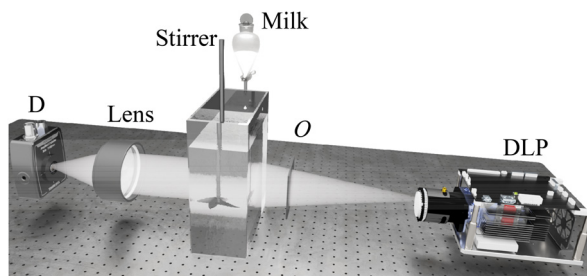
To verify the proposed CI in complex media, an experimental setup is shown in Fig. 1. A digital light projector (Texas Instruments, DLP4710EVM-LC) including a RGB LED light source and a digital micromirror device (DMD) sequentially projects random patterns with 128×128 pixels onto an object, which is placed in front of complex media. To generate complex media, a certain volume of milk solution is continuously dropped into a transparent water tank with dimensions of 15.0 cm (length) × 10.0 cm (width) × 30.0 cm (height), which contains 3000-ml pure water. The milk solution composed of 200-ml pure water and different volumes of milk is added into a separate funnel before each experiment. During the measurement, a stirrer keeps rotating at a constant rotational speed to generate dynamic media. Light fields carrying object information are scrambled completely after propagating through complex media and collected by a lens with a focal length of 10.0 cm. Then, a single-pixel detector (Thorlabs, PDA100A2) is utilized to detect light intensities with resultant photocurrents measured by a data acquisition device (ART technology, USB8586). Finally, the detected intensities and illumination patterns are used to retrieve object information.

Figure 2 shows a schematic of the proposed CI in complex media with varying thresholds and 1-bit sensing. Random patterns $P_i\,(i = 1, \ldots, m)$ are sequentially projected onto an object O by using a digital light projector. The transmitted light propagates through complex media and then collected by a single-pixel detector, which can be described by

$$\tilde{s}_i = k_i s_i = k_i \sum_{(x,y)} P_i O, \tag{1}$$

where s_i and $\tilde{s}_i$ denote light intensities, respectively, recorded in free space and complex media and (x, y) represents 2D spatial coordinate. It can be seen that an unknown scaling factor k_i is coupled into the light intensity recorded in complex media, leading to an extra fluctuation in the recorded light intensity.

In this case, the scaling factors vary dramatically during the measurement, which fails object reconstruction in conventional CI. The unknown scaling factors cause large fluctuations in light intensities, which cannot be eliminated by a constant threshold. Hence, to eliminate dynamic scaling factors, varying thresholds are utilized here to flexibly binarize light intensities. It has been demonstrated[24] that light intensities recorded in free space satisfy a Gaussian distribution with

FIG. 1. A schematic experimental setup for the proposed CI in complex media with varying thresholds and 1-bit compressive sensing. D, single-pixel detector; DLP, digital light projector; and O, object.
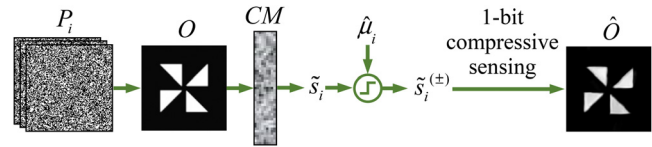
FIG. 2. A schematic of the proposed CI in complex media with varying thresholds and 1-bit compressive sensing. P_i, the ith illumination pattern; CM, complex media; $\tilde{s}_i$, single-pixel intensity with ith illumination pattern; $\hat{\mu}_i$, the ith estimated varying threshold; $\tilde{s}_i^{(\pm)}$, binarized light intensity using the estimated varying threshold; $\hat{O}$, a finally reconstructed correspondence image.

an expectation μ and a standard deviation σ. Based on Eq. (1), it can be shown that light intensities recorded in complex media can be described by

$$\begin{aligned} p(\tilde{s}_i) &= \mathcal{N}(\tilde{s}_i|\mu_i, \sigma_i^2) \\ &= \mathcal{N}(\tilde{s}_i|k_i\mu, k_i^2\sigma^2), \end{aligned} \tag{2}$$

where $\mathcal{N}(\cdot)$ denotes a Gaussian distribution, $p(\cdot)$ denotes the probability density function of a random variable, and μ_i and σ_i denote expectation and standard deviation in the CI through complex media, respectively. In Eq. (2), it can be seen that dynamic scaling factors are coupled into expectations of unknown Gaussian distributions, which can be estimated as varying thresholds. A probabilistic model is built to find estimations that can best fit the light intensities recorded in complex media via maximizing the log-likelihood distribution described by

$$\hat{\mu}_i, \hat{\sigma}_i = \arg\max_{\mu_i, \sigma_i} \log \prod_{i=1}^{m} p(\tilde{s}_i|\mu_i, \sigma_i). \tag{3}$$

The optimization model in Eq. (3) can be solved by a Gaussian process regression algorithm.[25] The estimated expectations $\hat{\mu}_i$ are utilized to represent μ_i as varying thresholds to binarize the light intensities recorded in complex media. It can be illustrated that the binarized intensities based on varying thresholds in complex media are equivalent to the binarized ones based on a constant threshold in free space, which can be described by

$$\tilde{s}_i^{(\pm)} = \begin{cases} +1, & \tilde{s}_i \geq \mu_i \\ -1, & \tilde{s}_i < \mu_i \end{cases} \rightarrow \begin{cases} +1, & k_i s_i \geq k_i \mu \\ -1, & k_i s_i < k_i \mu \end{cases} = \begin{cases} +1, & s_i \geq \mu, \\ -1, & s_i < \mu. \end{cases} \tag{4}$$

It is given in Eq. (4) that the varying thresholds can effectively eliminate dynamic scaling factors. On the contrary, the constant threshold ignores intrinsic distributions in light intensities recorded in complex media, which causes blind binarization and fails object reconstruction in conventional CI. Based on the binarized intensities, the threshold operation also separates illumination patterns into two groups, each of which can generate one reconstruction by superimposing illumination patterns belonging to it,

$$\tilde{O}_+ = \sum_i P_i, i \in \left\{i|\tilde{s}_i^{(\pm)} = +1\right\}, \tag{5}$$

$$\tilde{O}_- = \sum_i P_i, i \in \left\{i|\tilde{s}_i^{(\pm)} = -1\right\}. \tag{6}$$

Reconstruction based on Eq. (6) shows an opposite grayscale distribution to object transmittance, which is termed a negative image,

11 September 2024 08:11:14

while reconstruction based on Eq. (5) is called as a positive image. A correspondence image with a higher contrast can be obtained by subtracting the negative image from the positive image, which can be described by

$$\tilde{O} = \tilde{O}_+ - \tilde{O}_-. \qquad (7)$$

It should be noted that object reconstruction based on Eqs. (5)–(7) suffers from poor quality. From a probabilistic view, a correspondence image in Eq. (7) can be considered as a sample from a Gaussian distribution with the expectation linear to object transmittance. Any sample from the Gaussian distribution may fluctuate around the object transmittance, causing a noise-like characteristic in the correspondence image. To tackle this problem, here, we propose a modified 1-bit compressive sensing algorithm. The key function of 1-bit compressive sensing is to find an estimation of the unknown signal with minimal L1 norm and total variation (TV) norm based on binarized measurements,[26]

$$\hat{o} = \arg \min_{\|o\|_2 \leq 1} \left(-\frac{1}{m} \langle \tilde{o}, o \rangle + \lambda_1 \|o\|_1 + \lambda_2 \|o\|_{TV} \right), \qquad (8)$$

where $\tilde{o}$ denotes the vectorized result of $\tilde{O}$ in Eq. (7), λ_1 and λ_2, respectively, represent regularization parameters of L1 norm and TV norm, and $\hat{o}$ represents the vectorization of a final reconstruction.

The optimization model in Eq. (8) has a closed-form solution,

$$\hat{o} = \frac{\mathcal{P}_1(\mathcal{P}_2(\tilde{o}/m))}{\|\mathcal{P}_1(\mathcal{P}_2(\tilde{o}/m))\|_2}, \qquad (9)$$

where $\mathcal{P}_1(\cdot)$ and $\mathcal{P}_2(\cdot)$ are proximal operators of L1 norm and TV norm with the corresponding regularization parameters λ_1 and λ_2, respectively. The operator $\mathcal{P}_1(\cdot)$ has a closed-form solution, which can be described by

$$\mathcal{P}_1(x) = \text{sign}(x) \odot \max(|x| - \lambda_1, 0), \qquad (10)$$

where $\text{sign}(\cdot)$ returns the sign of its input and $\odot$ denotes the element-wise product. It is worth noting that the 1-bit compressive sensing algorithm can effectively reconstruct binary or grayscale objects.

In practice, reconstruction based on Eq. (9) may suffer from significant errors, since TV minimization is not robust under high noise level. As an advanced denoising algorithm, the block-matching and 3D filtering (BM3D)[27] algorithm can be used to replace the proximal operator for TV minimization with an iteration framework introduced to ensure stable reconstructions with high quality. With the L1 norm minimization and BM3D algorithm, object reconstruction with high fidelity can be realized. The detail of the proposed algorithm is given in Algorithm 1.

ALGORITHM 1.

1. **Input:** $\tilde{o}$, λ_1, and the total iteration number N
2. **Initialization:** Set the iteration count $k = 0$ and initial estimation $x^{(0)} = \tilde{o}$
3. For $k = 0 : N - 1$ do
      i) $x'^{(k)} = BM3D(x^{(k)})$
      ii) $x^{(k+1)} = \mathcal{P}_1(x'^{(k)})/\|\mathcal{P}_1(x'^{(k)})\|_2$
4. **Output:** Estimation $\hat{o} = x^{(N)}$

Figure 3 shows experimental results of a USAF 1951 resolution target (elements 4–6 of group −1 with the minimal linewidth of 561.23 μm) using conventional CI and the proposed method. The sampling ratio is 1.0, and diffraction limit of the CI system is measured as 258.75 μm based on the second-order correlation method[28] in this experiment. In Fig. 3(a), strong fluctuations, caused by dynamic scaling factors, can be observed in the single-pixel measurements. A constant threshold calculated by using normalized intensities is used for binarization. Since the constant threshold ignores the effect of dynamic scaling factors, effective information of the object cannot be retrieved from the binarized intensities, which can be seen in Figs. 3(b)–3(d). Therefore, varying thresholds are obtained to compensate for the fluctuations caused by dynamic scaling factors. In Fig. 3(e), varying thresholds are generated by solving the optimization model in Eq. (3). It can be seen that the generated thresholds show a similar trend with the measurements. Then, light intensities are binarized based on the varying thresholds with the binarized results utilized to reconstruct the unknown object. Figures 3(f) and 3(g) show positive and negative images obtained by superimposing the corresponding random patterns based on Eqs. (5) and (6), respectively. Compared with the results in Figs. 3(b) and 3(c), effective information of the unknown object can be observed, which verifies feasibility of the varying thresholds. It is also illustrated that a differential operation in Eq. (7) can obtain a correspondence image with higher contrast, which can be seen in Fig. 3(h). In addition, with the modified 1-bit compressive sensing algorithm, the reconstruction quality is enhanced as shown in Fig. 3(i). The element 6 of group −1 in USAF 1951 resolution target is well resolved.
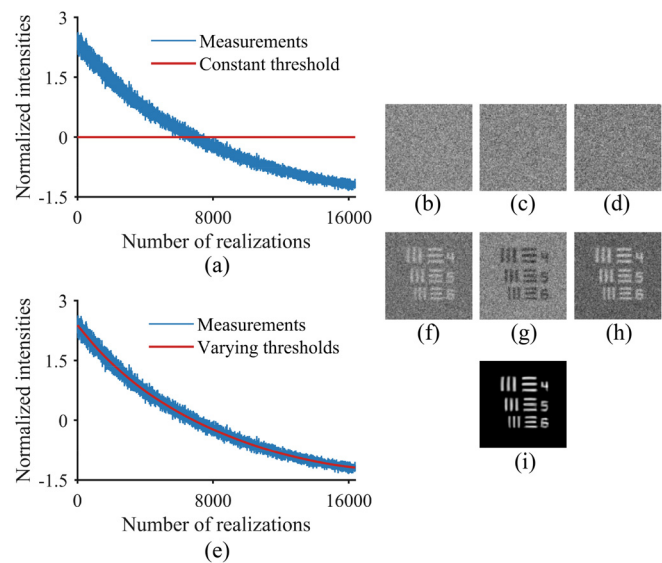
FIG. 3. Experimental results of USAF 1951 resolution target: (a) Normalized single-pixel light intensities and a constant threshold, (b)–(d) positive, negative, and correspondence images obtained by conventional CI with a constant threshold, (e) normalized single-pixel light intensities and the varying thresholds generated by the proposed method, (f)–(h) positive, negative, and correspondence images obtained by using the proposed CI with the generated varying thresholds, and (i) a finally reconstructed correspondence image obtained by using the proposed algorithm. Here, the normalization is performed by subtracting the average value from the directly measured intensities and then divided by the standard deviation.

The proposed method can eliminate dynamic scaling factors for high-resolution object reconstruction in complex media where conventional methods cannot work.

We apply the proposed method for experimentally testing different objects using different sampling ratios, as shown in Fig. 4. The objects 1 and 2 are fabricated by leveraging 3D printing with dimensions of $1.7 \times 1.7\,\text{cm}^2$ and $1.4 \times 1.4\,\text{cm}^2$, respectively. The object 3 is element 1 of group -2 (the linewidth of $2000\,\mu$m) in USAF 1951 resolution target. The experimental results of object 1 can be seen in Figs. 4(a)–4(e) with a sampling ratio of 0.2, 0.4, 0.6, 0.8, and 1.0, respectively. It is observed that the finally reconstructed correspondence images are of high quality when the sampling ratio is greater than or equal to 0.4. Although the quality of the final reconstruction result degrades with a sampling ratio of 0.2, features of the object are still well preserved. Similar results can be observed for objects 2 and 3, as shown in Figs. 4(f)–4(j) and 4(k)–4(o), respectively. Hence, the proposed method is experimentally verified to achieve object reconstruction with high fidelity in complex media under low sampling ratios.

To quantitatively evaluate the proposed method, we explore influence of rotational speed of the stirrer and volumes of milk on quality of the finally reconstructed correspondence images, i.e., contrast-to-noise ratio (CNR),[29,30] which is given by

$$\text{CNR} = \frac{2(\mu_s - \mu_b)}{(\sigma_s + \sigma_b)}, \qquad (11)$$

where μ_s and μ_b, respectively, denote average intensities in signal part (area of interest) and background part of a finally reconstructed correspondence image, and σ_s and σ_b represent standard deviations in signal part and background part, respectively. Experimental results are shown in Fig. 5. In Fig. 5(a), when rotational speed of the stirrer increases from 400 to 1000 rpm, a slight decrease in CNR values can be observed at each specific sampling ratio ranging from 0.4 to 1.0. When the rotational speed of the stirrer reaches 1000 rpm with a sampling ratio of 0.2, the CNR value reaches a minimum since the portion of binarization errors increases significantly. In Fig. 5(b), when the volume of the milk dropped into water tank increases from 10 to 40 ml, CNR values decrease with different extents. Similar to the case of
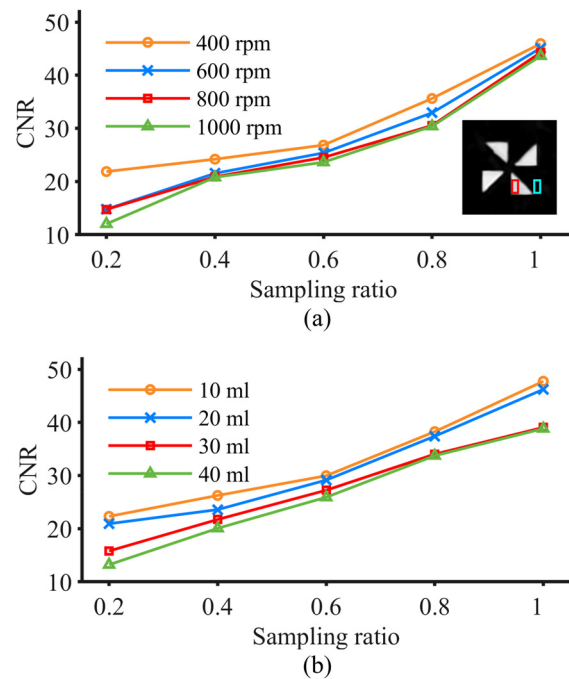
FIG. 5. (a) Influence of rotational speed of the stirrer on the CNR of the finally reconstructed correspondence images obtained by the proposed method, and (b) influence of the volume of the milk on the CNR of the finally reconstructed correspondence images obtained by the proposed method. The inset shows signal part (red box) and background part (cyan box) for CNR calculations.

rotational speed, the CNR value reaches the lowest level with a sampling ratio of 0.2 when 40-ml milk is added because of the highest portion of binarization errors. In addition, it can be seen that the sampling ratio results in a larger variation in CNR values than other parameters. It is experimentally verified that the proposed method shows high robustness against different parameters of complex media.

In conclusion, we report and experimentally verify high-fidelity CI in complex media with varying thresholds and 1-bit compressive sensing. To eliminate dynamic scaling factors, light intensities recorded in complex media are binarized with varying thresholds. Compared with CI with a constant threshold, the proposed varying thresholds can effectively eliminate the scaling factors. Then, the binarized intensities and illumination patterns can be utilized to retrieve object information using a modified 1-bit compressive sensing algorithm. Experimental results verify that the proposed method can realize object reconstruction with high fidelity, low sampling ratio, and high robustness under different settings of complex media. Since complex media impose dynamic scaling factors which can be eliminated by our method, prospect of potential applications can be provided for CI in various complex media, such as turbid water, thick tissues, and dynamic smoke as well as multiple complex media. Furthermore, the method can also be used in other imaging systems when dynamic scaling factors cause large fluctuations in measurements. In addition, the binarized intensities can facilitate high-efficiency transmission and storage owing to its insensitivity to non-linear distortions. Adaptive and real-time varying threshold generation scheme can be studied in the future.
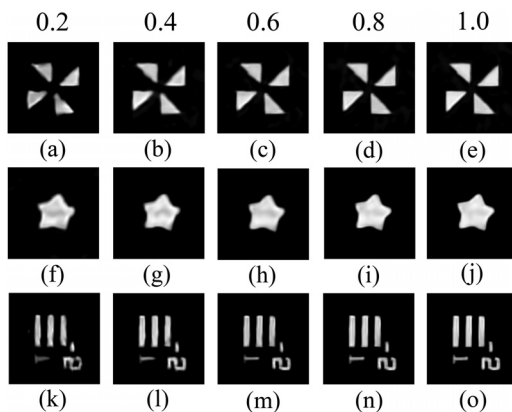
FIG. 4. The finally reconstructed correspondence images obtained by using the proposed method: (a)–(e) object 1, (f)–(j) object 2, and (k)–(o) object 3 under different sampling ratios (0.2, 0.4, 0.6, 0.8, and 1.0, respectively).

AUTHOR DECLARATIONS

Conflict of Interest

The authors have no conflicts to disclose.

Author Contributions

Zhihan Xu: Conceptualization (lead); Investigation (lead); Writing – original draft (lead). **Qian Song:** Investigation (supporting). **Wen Chen:** Conceptualization (lead); Methodology (lead); Supervision (lead); Writing – review & editing (lead).

DATA AVAILABILITY

The data that support the findings of this study are available from the corresponding author upon reasonable request.

REFERENCES

[1] M. P. Edgar, G. M. Gibson, and M. J. Padgett, Nat. Photonics **13**, 13 (2019).

[2] B. I. Erkmen and J. H. Shapiro, Adv. Opt. Photonics **2**, 405 (2010).

[3] G. M. Gibson, S. D. Johnson, and M. J. Padgett, Opt. Express **28**, 28190 (2020).

[4] N. Radwell, K. J. Mitchell, G. M. Gibson, M. P. Edgar, R. Bowman, and M. J. Padgett, Optica **1**, 285 (2014).

[5] Y. Liu, J. Suo, Y. Zhang, and Q. Dai, Opt. Express **26**, 32451 (2018).

[6] Z. Du, W. Zhao, A. Zhai, Z. Zhang, and D. Wang, Appl. Phys. Lett. **123**, 033702 (2023).

[7] K. Ota and Y. Hayasaki, Opt. Lett. **43**, 3682 (2018).

[8] G. Qu, X. Meng, Y. Yin, H. Wu, X. Yang, X. Peng, and W. He, Opt Lasers Eng. **137**, 106392 (2021).

[9] A. Vega, S. Saravi, T. Pertsch, and F. Setzpfandt, Appl. Phys. Lett. **117**, 094003 (2020).

[10] C. Moodley and A. Forbes, Sci. Rep. **12**, 10346 (2022).

[11] K. Luo, B. Huang, W. Zheng, and L. Wu, Chin. Phys. Lett. **29**, 074216 (2012).

[12] M. Li, Y. Zhang, X. Liu, X. Yao, K. Luo, H. Fan, and L. Wu, Appl. Phys. Lett. **103**, 211119 (2013).

[13] S. Yoon, M. Kim, M. Jang, Y. Choi, W. Choi, S. Kang, and W. Choi, Nat. Rev. Phys. **2**, 141 (2020).

[14] C. Wang, R. Liu, D. E. Milkie, W. Sun, Z. Tan, A. Kerlin, T. Chen, D. S. Kim, and N. Ji, Nat. Methods **11**, 1037 (2014).

[15] J. Park, Z. Yu, K. Lee, P. Lai, and Y. Park, APL Photonics **3**, 100901 (2018).

[16] X. Dang, N. M. Bardhan, J. Qi, L. Gu, N. A. Eze, C. Lin, S. Kataria, P. T. Hammond, and A. M. Belcher, Sci. Rep. **9**, 3873 (2019).

[17] W. Feng, Y. Yi, S. Li, Z. Xiong, B. Xie, and Z. Zeng, Opt. Commun. **552**, 130106 (2024).

[18] H. Zhan, Y. Peng, B. Chen, L. Wang, W. Wang, and S. Zhao, Opt. Express **30**, 23305 (2022).

[19] L. Zhou, Y. Xiao, and W. Chen, Appl. Phys. Lett. **123**, 011107 (2023).

[20] F. Li, M. Zhao, Z. Tian, F. Willomitzer, and O. Cossairt, Opt. Express **28**, 17395 (2020).

[21] D. Huyan, N. Lagrosas, and T. Shiina, APL Photonics **7**, 086104 (2022).

[22] W. Wan, C. Luo, F. Guo, J. Zhou, P. Wang, and X. Huang, Opt Laser Technol. **154**, 108346 (2022).

[23] Y. Xiao, L. Zhou, and W. Chen, Opt. Lett. **47**, 3692 (2022).

[24] J. Leng, W. Yu, and S. Wang, Phys. Rev. A **101**, 033835 (2020).

[25] C. K. Williams and C. E. Rasmussen, *Gaussian Processes for Machine Learning* (MIT Press, Cambridge, 2006).

[26] J. Hou and X. Liu, IEEE Access **10**, 116473 (2022).

[27] K. Dabov, A. Foi, V. Katkovnik, and K. Egiazarian, IEEE Trans. Image Process. **16**, 2080 (2007).

[28] F. Wang, C. Wang, M. Chen, W. Gong, Y. Zhang, S. Han, and G. Situ, Light **11**, 1 (2022).

[29] B. Redding, M. A. Choma, and H. Cao, Nat. Photonics **6**, 355 (2012).

[30] Y. Peng and W. Chen, Opt. Lett. **48**, 4480 (2023).